X-ray excited 3.2 eV luminescence from amorphous silica: radiative electron relaxation through an unidentified centre and its thermal switching

2008 J. Phys.: Condens. Matter 20 255249

(http://iopscience.iop.org/0953-8984/20/25/255249)

J. Phys.: Condens. Matter **20** (2008) 255249 (5pp) doi:10.1088/0953-8984/20/25/255249

X-ray excited 3.2 eV luminescence from amorphous silica: radiative electron relaxation through an unidentified centre and its thermal switching

Masashi Ishii[1], **Tomoko Yoshida**[2] **and Kenji Sakurai**[1]

[1] National Institute for Materials Science, 1-2-1 Sengen, Tsukuba 305-0047, Japan
[2] Department of Materials, Physics and Energy Engineering, Nagoya University, Nagoya 464-8603, Japan

Received 14 April 2008, in final form 7 May 2008
Published 28 May 2008
Online at stacks.iop.org/JPhysCM/20/255249

Abstract
We analyse the electron transition in amorphous silica by observing its soft x-ray excited optical luminescence (XEOL) and find an unidentified optical centre that electronically interacts with well-known defect sites in the radiative relaxation process. We propose an electronic state diagram and use it to illustrate the relaxation process in which electrons are transferred from an oxygen-deficiency centre emitting a 2.6 eV XEOL to an unidentified centre emitting a 3.2 eV XEOL in a temperature range of 85 to 200 K. By selecting an appropriate temperature to avoid the interaction between these centres, we can thermally switch the optical emission site, which is advantageous to the site-selective analysis of the XEOL.

1. Introduction

The photoluminescence (PL) of amorphous silica to be used in Si-based optical devices has been actively investigated over many years [1]. Visible PL emissions at energies of ∼1.9 and ∼2.6 eV are commonly observed and are known to be caused by defects in amorphous silica [2–4]. The following are valid models of the optically active defects: (1) a non-binding oxygen hole centre (NBOHC) representing a dangling-bond-type defect for the 1.9 eV PL [5] and (2) an oxygen-deficiency centre, most commonly denoted by ODC(II) representing an oxygen-vacancy-type defect for the 2.6 eV PL [6]. Photon absorption in the ultraviolet (UV) region, which excites these defect centres, has already been characterized by many researchers; therefore, this paper does not attempt to comment on the UV excitation and optical relaxation at each defect centre.

In this paper, we discuss an unidentified visible luminescence at 3.2 eV emitted from amorphous silica. This luminescence is not considered to be caused by pure amorphous silica; rather, it is generally accepted to be a Ge–impurity-related emission; a Ge impurity is considered to produce another oxygen-deficiency centre termed Ge(ODC) [7, 8]. However, in several papers, researchers have reported the emission of the 3.2 eV PL from pure silica and an electron transition band at this energy. (1) In experiments on UV-excited PL, Anedda *et al* have observed the 3.2 eV PL emitted from an amorphous silica sample in which Ge doping is unintentional [9]. They have reported that the Ge impurity contained in the sample is at most 1 ppm. They have found that the 3.2 eV PL is significant at room temperature, while the 2.6 eV PL emitted from the ordinary ODC(II) is superior at a low temperature of 10 K [10]. (2) Tohmon *et al* have observed the 3.2 eV PL in an optical fibre with a pure silica core when the fibre is excited via a $B_2\beta$ band of ∼5 eV [11]. They have not mentioned the amount of Ge impurity in the silica core fabricated by a soot process; however, it is clear that the Ge doping of the sample is not deliberate. (3) Paleari *et al* have investigated the UV-excited PL of stishovite, which is high-density crystal phase silica, and they have observed the 3.2 eV PL emitted from stishovite [12]. Although the optical property of crystal silica cannot be directly correlated to that of amorphous silica, the result suggests the possibility of the existence of some local Si–O structure that is independent of the surrounding crystallinity and has a common optical transition at 3.2 eV. They considered it to be a defect site such as a twofold-coordinated Si in the sixfold-coordinated structure of stishovite. (4) The 2.6 eV

PL is caused by the optical transition from the triplet state to the singlet state ($T_1 \rightarrow S_0$) in ODC(II). Skuja has found that the direct excitation $S_0 \rightarrow T_1$ has an absorption peak at ~3.2 eV, indicating an optical transition band at this energy [6]. Therefore, the minimization of the electron energy loss in the T_1 excitation state possibly causes a shift in the PL energy from 2.6 to 3.2 eV.

In this study, we confirm the unidentified 3.2 eV PL emitted from pure amorphous silica excited by synchrotron x-rays. The temperature dependence of luminescence intensity indicates a unique thermal quenching property and suggests the interaction of the unidentified centre with the other well-known defect centres NBOHC and ODC(II).

Unlike conventional PL, x-ray excited optical luminescence (XEOL) utilizes inner-shell excitations rather than valence-shell excitations. In fact, we use the excitation from the Si 1s state to the Si 3p state, indicating the extension of the excitation process from an interband transition to an interorbital transition. In general, the inner-shell excitation that induces photoelectron emission results in the formation of core holes. The occupation of the core holes by outer-shell electrons, which causes x-ray fluorescence or results in Auger electrons, is known to be the main relaxation process. However, subsequent relaxation is actually induced in a valence shell, resulting in XEOL. This extended photoexcitation provides additional information that is directly related to the molecular orbital composing the optically active centres [13, 14]. Moreover, in the case that synchrotron radiation, i.e. intense x-rays with selectable photon energy, is used for the excitation, x-ray absorption spectroscopy (XAS) can be carried out by monitoring XEOL, for elucidating the electronic states and local structure. The XEOL intensity as a function of the x-ray photon energy provides site-selective XAS spectra of the optically active site. We believe that an appropriately selected temperature condition in the XEOL measurement controls the electronic interaction between the unidentified site and the well-known defects NBOHC and ODC(II), switches the relaxation path, and effectively extracts the unidentified 3.2 eV XEOL.

2. Experiment

We performed the XEOL experiment [15, 16] at the UVSOR-II synchrotron radiation facility at the Institute of Molecular Science in Aichi prefecture, Japan. In the BL1A beamline [17], the synchrotron radiation was monochromatized by a (111)-oriented InSb double crystal. The x-ray excitation energy was tuned at (1) 1834 eV, just below the Si K-edge energy level, (2) 1848 eV, corresponding to the energy level of the electron transition from Si 1s to 3p, and (3) 1858 eV, well above the Si K-edge energy level.

At 1834 eV, since the x-rays could not excite 1s electrons, only those electrons in shallower levels such as 2s or 2p or in the valence band could be excited. At 1848 eV, the x-ray absorption of amorphous silica was the strongest [18]. The intensity of the x-rays monitored using a copper mesh was about 1×10^9 photons $mm^2\ s^{-1}$. The beam size was 1 mm × 4 mm.

The sample was a low-hydroxide (OH) (<1 ppm) fused amorphous silica disk (T-2030) produced by Covalent Materials Corporation (formally known as Toshiba Ceramics Co., Ltd), Japan. The main impurities of amorphous silica were Al (8 ppm), Na (1 ppm), and K (1 ppm), and no Ge impurity was detected (<0.1 ppm). The disk diameter of 13 mm was sufficiently larger than the x-ray beam size, and the disk thickness was 2 mm greater than the maximum x-ray penetration depth considered in our experiments (cf 7.4 μm for silica at an x-ray energy of 1834 eV).

The sample was mounted in an ultrahigh vacuum (UHV) chamber, whose temperature was controlled from room temperature to 50 K by means of a cryostat. The XEOL emitted from the sample was focused on an imaging spectrograph (CP-200, Jobin Yvon) by a convex lens installed in the UHV chamber. The imaging spectrograph had a grating with a groove density of 200 grooves mm^{-1}, providing a wavelength resolution of less than 3.5 nm. After passing through the grating, the XEOL was observed using a multichannel detector (1455-700, EG&G Princeton Applied Research). The detected signals were converted to a XEOL spectrum using an optical multichannel analyser system (OMA-III, EG&G Princeton Applied Research). The spectrum data were calibrated with the transmission efficiency of all these optics.

3. Results and discussion

3.1. Unidentified luminescence from pure amorphous silica

Figure 1 shows the XEOL spectra as a function of the sample temperature, summarized in a three-dimensional (3D) plot. The x-ray excitation energies are (a) 1834, (b) 1848, and (c) 1858 eV. The vertical and horizontal axes represent the photon energy of the XEOL and the sample temperature, respectively. The colour scale of the spectra in figures 1(a)–(c) indicates that the intensity range of the XEOL emitted at all three excitation energies is the same. As shown in this figure, the photon energy and the intensity of the XEOL change remarkably for various combinations of the excitation energy and sample temperature. To elucidate this change further, we categorize the 3D XEOL spectra into the following three groups. Group I spectra have the highest-intensity XEOL over the photon energy range of 2.7–4.0 eV in the temperature region of $100 < T < 270$ K; group II spectra are observed at a photon energy of around 2.6 eV in the low-temperature region of $T < 70$ K; finally, group III spectra are observed at a photon energy of 1.7 eV and in the same temperature region as that for group I spectra.

Group I spectra can be characterized by an emission peak at 3.2 eV, denoted by $L_{3.2}$, and this emission peak is attributed to the unidentified luminescence from pure amorphous silica. Group II spectra can be characterized by an emission peak at 2.6 eV, denoted by $L_{2.6}$, and it is considered to be attributed to the well-known emission band resulting from ODC(II). Finally, in group III spectra, a sharp XEOL peak denoted by $L_{1.7}$ is observed at 1.7 eV, which is expected to be attributable to the NBOHC; this emission energy is slightly lower than the reported value of ~1.9 eV.

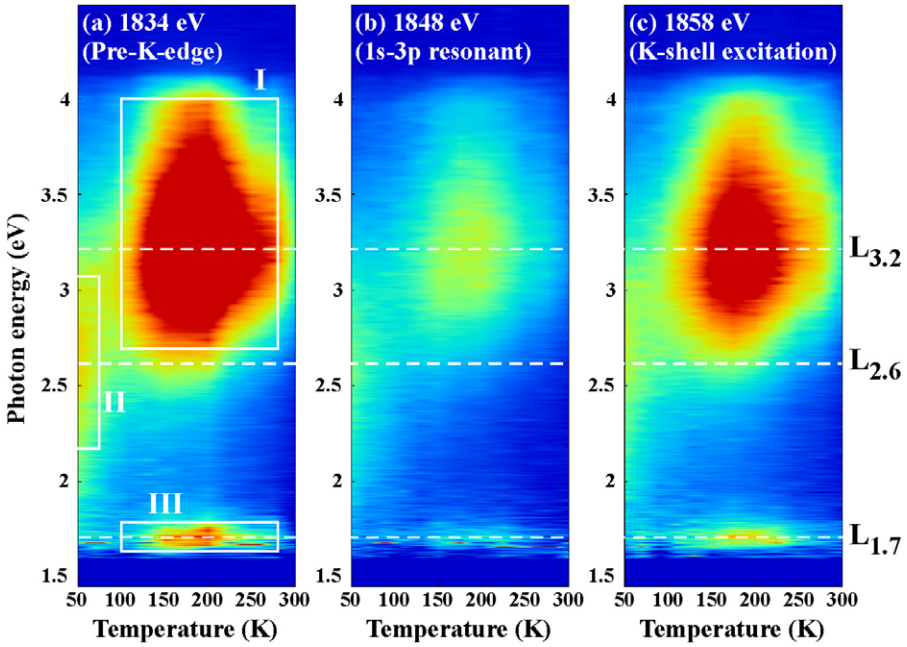

Figure 1. XEOL spectra as a function of sample temperature, summarized as a 3D plot. The x-ray excitation energies were (a) 1834, (b) 1848, and (c) 1858 eV.

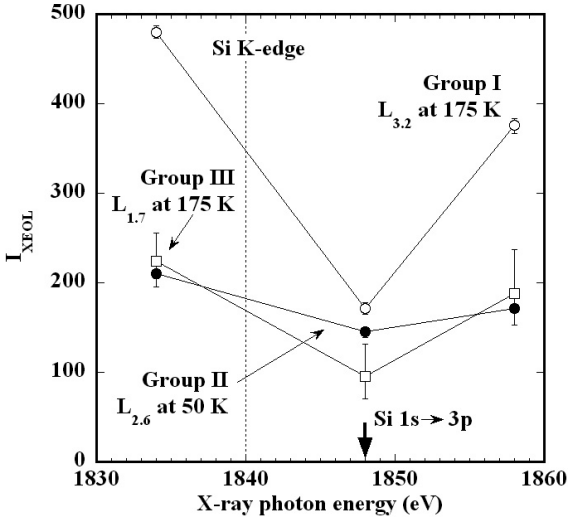

Figure 2. Intensities of XEOL emitted at 3.2 eV at 175 K (open circles), at 2.6 eV at 50 K (closed circles), and at 1.7 eV at 175 K (open squares) for distinctive x-ray excitation energies around the Si K-edge. Supplementary note: the error bar of $L_{2.6}$ is hidden in the closed circle.

The intensities of group I spectra strongly depend on the x-ray excitation energy, while group II spectra maintain an almost constant intensity that is independent of the x-ray excitation energy. These behaviours are quantitatively summarized in figure 2, in which open and closed circles denote the XEOL intensity I_{XEOL} as a function of the x-ray photon energy for $L_{3.2}$ at 175 K and for $L_{2.6}$ at 50 K, respectively. In this figure, I_{XEOL} of $L_{1.7}$ at 175 K with respect to the x-ray photon energy is also indicated by open squares. Although I_{XEOL} of $L_{1.7}$ has an insufficient signal-to-noise ratio for the low transmission efficiency of the optics, it would maintain about half intensity of $L_{3.2}$ within the x-ray photon energy range from (a) to (c); $L_{1.7}$ and $L_{3.2}$ have the same dependence on the x-ray excitation energy. To avoid misunderstanding of the data, we supplementary note that the error bar of $L_{2.6}$ is hidden in the plot of closed circles. The different behaviours of $L_{2.6}$ from $L_{3.2}$ and $L_{1.7}$ indicate distinctive hybridizations of the Si 3p orbital at each emission centre; the hybridization of the unidentified centre with Si 3p should be stronger than that of ODC(II) with Si 3p.

3.2. Electronic interactions of NBOHC and ODC(II) with the unidentified centre

Interestingly, the 3D XEOL spectra shown in figure 1 reveal that group II spectra are alternated with groups I and III spectra at ∼85 K. Moreover, groups I and III spectra exhibit an intensity peak at ∼200 K and shift to other states above this temperature. These transitions suggest electronic interactions of NBOHC and ODC(II) with the unidentified centre. The alternation at 85 K and the transition at 200 K, i.e. 'thermal switching', can be used for the selective detection of the XEOL. From figure 3, it is clear that the electronic state diagram and electron transition process are able to explain the temperature switching consistently. A sufficiently high energy of x-rays partly induces electron excitation and the subsequent relaxation to the T_1 state via the S_1 state of ODC(II) [6], denoted by (a) in figure 3. The electron transition processes after (a) are described as follows.

(1) At the boundary temperature of 85 K, the excited electrons in the T_1 state of $L_{2.6}$ overcome the potential barrier of $E_{85\ \mathrm{K}}$ and move into the excited states of $L_{3.2}$, as indicated

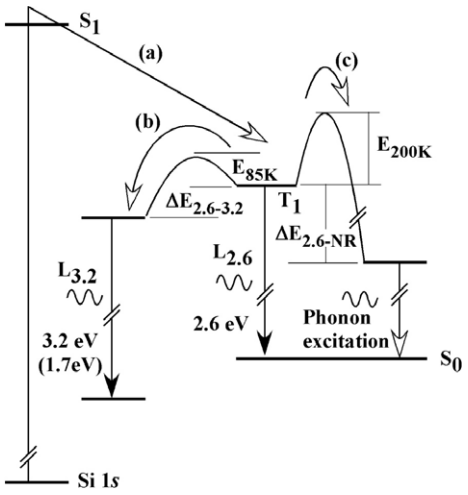

Figure 3. Electronic state diagram and electron transition process, including the unidentified optical centre.

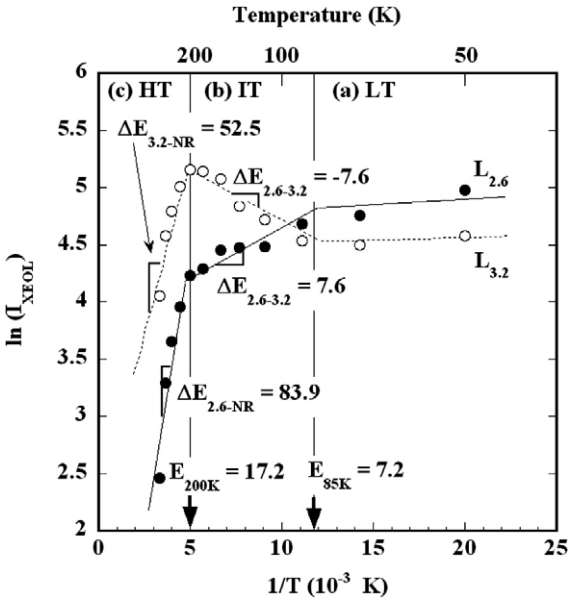

Figure 4. Arrhenius plot of XEOL intensity for 1848 eV excitation, which determines the energy levels indicated in figure 3. The values are expressed in meV.

by (b) in figure 3. The excited state of $L_{3.2}$ is lower than T_1 of $L_{2.6}$ by $\Delta E_{2.6-3.2}$. This electron transfer from $L_{2.6}$ to $L_{3.2}$ becomes more significant as the temperature increases; as a result, I_{XEOL} of $L_{2.6}$ decreases and that of $L_{3.2}$ increases.

(2) When the sample temperature becomes equal to another boundary temperature of 200 K, the excited electrons in T_1 of $L_{2.6}$ find a new relaxation path, as indicated by (c) in figure 3, because they have sufficient energy to overcome the higher potential barrier of $E_{200\,\mathrm{K}}$. The electrons drop to a lower-energy level, where the energy difference is $\Delta E_{2.6-\mathrm{NR}}$. This level leads to nonradiative relaxation, resulting in a decrease in I_{XEOL} of $L_{2.6}$.

(3) In the high-temperature region greater than 200 K, electrons introduced by process (b) in the excited state of $L_{3.2}$ are limited by the new nonradiative relaxation path described in (2). Therefore, the luminescence intensity of $L_{3.2}$ also decreases.

For more quantitative determination of the energy levels, we analyse the 3D XEOL spectra for the 1848 eV photon excitation shown in figure 1(b). At this excitation energy level, unlike at the excitation energy levels of 1834 and 1858 eV, $L_{3.2}$ and $L_{2.6}$ have a moderate intensity; therefore, we are able to analyse them independently without using artificial deconvolution processes.

Figure 4 shows the I_{XEOL} values of $L_{3.2}$ (open circles) and $L_{2.6}$ (closed circles) with respect to the temperature. In this figure, the vertical and horizontal axes represent the logarithmic XEOL intensity $\ln(I_{\mathrm{XEOL}})$ and the inverse of the temperature, $1/T$, respectively, yielding an Arrhenius plot. As shown in this figure, we can divide the plot into three regions: (a) a low-temperature (LT) region of $T < 85$ K with little or no variation in I_{XEOL} for both $L_{2.6}$ and $L_{3.2}$; (b) an intermediate-temperature (IT) region of 85 K $< T <$ 200 K in which an increase in temperature causes an increase in $L_{3.2}$ and a decrease in $L_{2.6}$; and (c) a high-temperature (HT) region of $T > 200$ K with rapidly decreasing $L_{3.2}$ and $L_{2.6}$.

The boundary temperatures for each region (85 and 200 K) shown in figure 4 can be converted into $E_{85\,\mathrm{K}}$ and $E_{200\,\mathrm{K}}$, shown in figure 3, by the factor kT, where k is the Boltzmann constant; then, $E_{85\,\mathrm{K}} = 7.2$ meV and $E_{200\,\mathrm{K}} = 17.2$ meV. To evaluate $\Delta E_{2.6-3.2}$ and $\Delta E_{2.6-\mathrm{NR}}$ shown in figure 3, we use the equation for the activation energy E_{a}, $\ln(I_{\mathrm{XEOL}}) = E_{\mathrm{a}}/kT$. Here, E_{a} equals $\Delta E_{2.6-3.2}$ and $\Delta E_{2.6-\mathrm{NR}}$ for the IT and HT regions, respectively.

For the IT region (b) shown in figure 4, we find that the intensity slopes of $L_{2.6}$ and $L_{3.2}$ in the Arrhenius plot $\mathrm{d}I_{\mathrm{XEOL}}/\mathrm{d}(1/T)$ have the same absolute value of $E_{\mathrm{a}} = 7.6$ meV but different signs with respect to $1/T$; $\mathrm{d}I_{\mathrm{XEOL}}/\mathrm{d}(1/T)$ of $L_{2.6}$ has a positive sign, while that of $L_{3.2}$ has a negative sign. This result is natural for the electron transfer from $L_{2.6}$ to $L_{3.2}$, which is shown in figure 3. The calculated value of $E_{\mathrm{a}} = \Delta E_{2.6-3.2} = 7.6$ meV indicates that the excited states of $L_{2.6}$ and $L_{3.2}$ are extremely close and coupled with a very low potential barrier of $E_{85\,\mathrm{K}} = 7.2$ meV. Therefore, even in the LT region, the excited electrons should swiftly jump from $L_{2.6}$ to $L_{3.2}$. However, the experimental results indicate that the preferred radiative path for $L_{2.6}$ is accessible in the LT region only. This suggests that the $L_{2.6}$ excitation state has a short lifetime, which is in agreement with the findings by Anedda *et al* [9].

In the HT region (c), excited electrons with a thermal energy of $E_{200\,\mathrm{K}} = 17.2$ meV find a nonradiative transition path, resulting in their relaxation to the ground state S_0 without emission. On the analogy of $\Delta E_{2.6-\mathrm{NR}}$, the intensity decay of $L_{3.2}$, i.e. $\Delta E_{3.6-\mathrm{NR}}$, can be quantitatively evaluated from the $\mathrm{d}I_{\mathrm{XEOL}}/\mathrm{d}(1/T)$ value of $L_{3.2}$ in the Arrhenius plot shown in figure 4. The $\Delta E_{3.6-\mathrm{NR}}$ value of 52.5 meV is roughly two-thirds of the $\Delta E_{2.6-\mathrm{NR}}$ value of 83.9 meV. This is due to the other relaxation path yielding $L_{1.7}$ (see figure 2).

In contrast to the alternate correlation of $L_{2.6}$ with $L_{3.2}$, $L_{1.7}$ is synchronized with $L_{3.2}$, as shown in the 3D XEOL spectra in figure 1 and their numerical analyses in figure 2. The synchronization mechanism of $L_{1.7}$ is unclear at this stage. However, the symmetry between $L_{2.6}$ and $L_{1.7}$ suggests contrasting transition paths of the electrons of ODC(II) and NBOHC. Considering the small energy barrier observed in figure 4, we do not deny the possibility of temporary x-ray irradiation damage changing ODC(II) to quasi-NBOHC, which is accompanied by the formation of $L_{3.2}$. Detailed optical properties observed with ordinary PL will be discussed elsewhere.

An independent relaxation at each site is the electron transition process required for site-selective XAS in which XEOL is monitored. From the model discussed in figures 3 and 4, we can clearly observe that the interactive relaxation in the IT region cannot provide site selectivity. For the selective observation of $L_{2.6}$, the LT region should be used as an experimental condition because of the preferred radiative path. On the other hand, for $L_{3.2}$, the HT region is favourable for experimentation because of the absence of $L_{2.6}$, caused by the nonradiative relaxation, as indicated in figure 3(c). The larger decay of $\Delta E_{2.6-\mathrm{NR}} > \Delta E_{3.2-\mathrm{NR}}$ indicates that a high temperature is more favourable for site selection.

4. Summary

In summary, we have prepared an electronic state diagram of the defects in amorphous silica, which consistently explains the results of the XEOL experiments that show the emission of the unidentified luminescence at 3.2 eV. In the IT range of $85 < T < 200$ K, defects with 2.6 eV PL and 3.2 eV PL are concurrently relaxed because of an interactive process. For the selective analyses of these defects, we have determined that thermal switching between the 2.6 eV PL and the 3.2 eV PL can be induced as follows. In the LT region of temperatures less than 85 K, rapid radiative relaxation prior to the interaction induces the emission at 2.6 eV; in the HT region of temperatures greater than 200 K, nonradiative relaxation eliminates the emission at 2.6 eV, resulting in a dominant emission at 3.2 eV.

References

[1] For example Skuja L 1998 *J. Non-Cryst. Solids* **239** 16
[2] Anedda A, Bongiovanni G, Cannas M, Conglu F, Mura A and Martini M 1993 *J. Appl. Phys.* **74** 6993
[3] Nishikawa H, Watanabe E, Ito D, Takiyama M, Ieki A and Ohki Y 1995 *J. Appl. Phys.* **78** 842
[4] Kucheyev S O and Demos S G 2003 *Appl. Phys. Lett.* **82** 3230
[5] Stapelbroek M, Griscom D L, Friebele E J and Sigel G H Jr 1979 *J. Non-Cryst. Solids* **32** 313
[6] Skuja L 1994 *J. Non-Cryst. Solids* **167** 229
[7] Skuja L N, Trukin A N and Plaudis A E 1984 *Phys. Status Solidi* a **84** K153
[8] Agnello S, Boscaino R, Cannas M and Galardi F M 1998 *J. Non-Cryst. Solids* **232–234** 323
[9] Anedda A, Carbonaro C M, Clemente F and Corpino R 2002 *J. Appl. Phys.* **92** 3034
[10] Anedda A, Carbonaro C M, Corpino R and Raga F 1998 *Nucl. Instrum. Methods Phys. Res.* B **141** 719
[11] Tohmon R, Mizuno H, Ohki Y, Sasagane K, Nagasawa K and Hama Y 1989 *Phys. Rev.* B **39** 1337
[12] Paleari A, Chiodini N, Di Martino D and Meinardi F 2003 *Phys. Rev.* B **68** 184107
[13] Goulon J, Tola P, Lemonnier M and Dexpert-Ghys J 1983 *Chem. Phys.* **78** 347
[14] Sham T K, Jiang D T, Coulthard I, Lorimer J W, Feng X H, Tan K H, Frigo S P, Rosenberg R A, Houghton D C and Bryskiewicz B 1993 *Nature* **363** 331
[15] Yoshida T, Tanabe T, Ii T and Yoshida H 2002 *Nucl. Instrum. Methods* B **191** 382
[16] Yoshida T, Tanabe T, Takahara S and Yoshida H 2005 *Phys. Scr.* T **115** 528
[17] Hiraya A, Horigome T, Okada N, Mizutani N, Sakai K, Matsudo O, Hasumoto M, Fukui K and Watanabe M 1992 *Rev. Sci. Instrum.* **63** 1264
[18] Sammynaiken R, Naftel S J, Sham T K, Cheah K W, Averboukh B, Huber R, Shen Y R, Qin G G, Ma Z C and Zong W H 2002 *J. Appl. Phys.* **92** 3000